Alexandria Engineering Journal 104 (2024) 665–679

Contents lists available at ScienceDirect

Alexandria Engineering Journal

journal homepage: www.elsevier.com/locate/aej

Original article

Broadband high gain performance MIMO antenna array for 5 G mm-wave applications-based gain prediction using machine learning approach

Md. Ashraful Haque [a], Md Sharif Ahammed [a], Redwan A. Ananta [a], Khaled Aljaloud [b], Noorlindawaty Md Jizat [c,*], Wazie M. Abdulkawi [d], Kamal Hossain Nahin [a], Samir Salem Al-Bawri [e,*]

[a] Department of Electrical and Electronic Engineering, Daffodil International University, Dhaka 1341, Bangladesh
[b] College of Engineering, Muzahimiyah Branch, King Saud University, Riyadh 11451, Saudi Arabia
[c] Faculty of Engineering, Multimedia University, Cyberjaya 62300, Malaysia
[d] Department of Electrical Engineering, College of Engineering in Wadi Addawasir, Prince Sattam bin Abdulaziz University, Al-Kharj 11991, Saudi Arabia
[e] Space Science Centre, Climate Change Institute, Universiti Kebangsaan Malaysia (UKM), Bangi 43600, Malaysia

A R T I C L E I N F O

Keywords:
MIMO
5G antenna
Machine learning
RLC equivalent

A B S T R A C T

This paper presents the findings about implementing a machine learning (ML) technique to optimize the performance of 5 G mm wave applications utilizing multiple-input multiple-output (MIMO) antennas operating at the 28 GHz frequency band. This article examines various methodologies, including simulation, measurement, and the utilization of an RLC-equivalent circuit model, to evaluate the appropriateness of an antenna for its intended applications. In addition to its compact dimensions, the proposed design exhibits a maximum gain of 10.34 dBi, superior isolation exceeding 26 dB, and a broad bandwidth of 16.56 % Centered at 28 GHz and spanning from 25.905 to 30.544 GHz. Another supervised regression machine learning technique is utilized to predict the antenna's gain accurately. Machine learning (ML) models can be assessed by several measures, such as the variance score, R square, mean square error (MSE), mean absolute error (MAE), root mean square error (RMSE), and Mean Absolute Percentage Error (MAPE). Among the six machine learning models considered, it is seen that the Gaussian Process Regression (GPR) model exhibits the lowest error and achieves the highest level of accuracy in forecasting gain. The antenna under consideration has promising qualities for its intended use in high-band 5 G applications. This is evidenced by the modelling findings obtained from Computer Simulation Technology (CST) and Advanced Design System (ADS)and the measured and projected results derived using machine learning methodologies.

1. Introduction

Microstrip patch antennas are standard antennas for microwave and wireless networks. Its portability and versatility stem from its tiny, straightforward design [1]. Microstrip patch antennas can take several forms, including square, circular, and octagonal designs. Patches come in various shapes, the most common of which is the rectangular patch [2]. In the case of microstrip patch antennas, adequate bandwidth and excellent impedance matching can be challenging to achieve. Increasing the bandwidth and perfecting the impedance match can be accomplished using slotting, parasitic components, and matching networks [3]. The antenna's impedance matching and bandwidth will change depending on the feed mechanism.

A microstrip 1×2 array antenna is a specific configuration of microstrip patch antennas operating as a two-element array. This microstrip patch antenna arrangement is called a 1×2 array [4]. This is accomplished by adjusting the relative phase and magnitude of the signals sent into each element. A straightforward illustration of an array configuration is provided by microstrip 1×2 array antennas [5]. There is a wide range of possible dimensions and configurations for arrays, such as linear, planar, and conformal arrays. The application and the kind of radiation pattern that is wanted both have a role in deciding which array configuration to use [6].

A 28 GHz 5 G MIMO antenna design has been modified to function solely inside the 28 GHz frequency band, focusing on the unique attributes of millimeter wave (mm-Wave) communications [7]. To achieve

* Corresponding authors.
E-mail addresses: noorlindawaty.jizat@mmu.edu.my (N.M. Jizat), s.albawri@gmail.com, samir@ukm.edu.my (S.S. Al-Bawri).

https://doi.org/10.1016/j.aej.2024.08.025
Received 6 February 2024; Received in revised form 5 August 2024; Accepted 6 August 2024
Available online 14 August 2024

multiple-input multiple-output (MIMO) capabilities, it is probable that the system would incorporate multiple antennas at both the sending and receiving terminals [8]. The antennas mentioned above are intended for data transmission and reception inside a 5 G network. This network provides potential for diverse applications [9], such as facilitating high-speed internet connectivity and enabling the interconnection of various devices within the Internet of Things (IoT) paradigm, among other possibilities.

Table 1 shows a review of different present endeavors in terms of their main ideas. The table compares things like working frequency, small size, bandwidth, gain, isolation, ECC, and CCL. It is also the smallest and has the widest bandwidth. The articles [10-16,18] indicate that CST has a gain of 8.3 dB, 9.24 dB, 6.5 dB, 6.9 dB, 8.2 dB, 8.6 dB, 9.53 dB, 10 dB, and 5 dB. However, CST has a gain of 10.34 dB.

In this paper, the proposed 4 port MIMO antenna array design has a bandwidth of 4.64 GHz. Authors have cited bandwidths at frequencies of 4.1 GHz, 2.1 GHz, 3 GHz, 0.4 GHz, 0.5 GHz, 1.5 GHz, 3.5 GHz, 3.5 GHz, and 7 GHz. The design under consideration has isolation levels exceeding 26.065 dB. The previously mentioned references include data on decibel values above 22 dB, 18 dB, 17 dB, 17 dB, 25 dB, 23.31 dB, 22 dB, 20 dB, and 25 dB, respectively. The MIMO antenna proposed exhibits outstanding performance attributes when compared to alternative choices, as evidenced by an extremely low ECC value of less than 0.0008 and a high DG value above 9.99. The utilization of the RLC equivalent circuit outcomes is not observed in the sources, yet they hold significant importance in the provided architecture. The architectural design under consideration extensively employs machine learning techniques; nonetheless, it is important to provide a more precise definition of this word within the pertinent literature.

2. Antenna geometry configuration

In this section, we have conducted an analysis of the proposed antenna design. Each phase of this design serves a distinct purpose to enhance performance. The single-element antenna's compact size may lead to bandwidth, gain, and efficiency limitations. We have developed an array that exhibits enhanced bandwidth, gain, and efficiency [19]. MIMO is the ultimate measure to augment the aggregate data rate, bolster system dependability, and enhance communication quality.

2.1. Single element

Fig. 1 shows the different steps of designing the single-element antenna. To begin designing the single-element antenna, the initial step involves the process of etching 0.035 mm of annealed copper onto a Rogers RT5880 substrate that has a thickness of 0.787 mm. This substrate is characterized by a dielectric constant of 2.2 and a loss tangent of 0.0009, both of which are critical parameters that determine the antenna's performance. The etching process is a crucial step that shapes the antenna's structure and prepares it for further processing. The dimensions of the substrate and patch are Ws×Ls and Wp×Lp, respectively. The feed has an impedance of 50 ohms to minimize the back reflections from the antenna to the input port and has a dimension of Wf×Lf. In this step, the resonant frequency and return loss were poor.

In the second step of the antenna design process, it is recommended to introduce two slots on the lower left and right sides of the antenna. These slots should have precise dimensions of Ws1 and Ls1, which have been determined to result in a significant improvement in the Reflection coefficient. By incorporating these slots into the design, the antenna's performance can be greatly enhanced. In the final step on the top of the patch, we introduced the third, fourth, and fifth slot, which has a dimension of Ws2×Ls2 and Ws3×Ls3, respectively. The antenna is

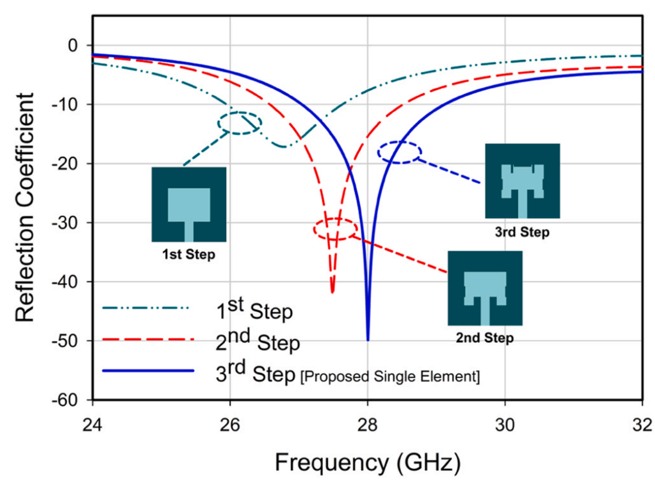

Fig. 1. Reflection coefficient of each step of the single element antenna.

Table 1
Performance comparisons with the published state of the art.

Ref	Resonance Frequency (GHz)	Frequency Range (GHz)	BW (GHz)	Size	No of port	Gain (dB)	Isolation (dB)	ECC, DG (dB)	Efficiency (%)	Substrate Material	RLC Circuit	ML Analysis
[10]	28	25.5–29.6	4.1	$2.8\lambda_0\times 3.26\lambda_0$	4	8.3	>22	0.01, 9.96	82	Rogers RO4350B	NO	NO
[11]	28	26.867–28.975	2.1	$1.86\lambda_0\times1.86\lambda_0$	4	9.24	>18	0.0013, NA	78.6	Rogers RT5880	NO	NO
[12]	28	26–29	3	$2.8\lambda_0\times2.8\lambda_0$	4	6.5	>17	0.0015, NA	90	Rogers RT5880	NO	NO
[13]	28	NA	0.4	$3.08\lambda_0\times 2.56\lambda_0$	2	6.9	>17	0.2, 9.7	87	TLY−5	NO	NO
[14]	28	27.8–28.3	0.5	$11.2\lambda_0\times5.6\lambda_0$	2	8.2	25	0.014, 9.99	85	Rogers RO4350	NO	NO
[15]	28	27.1–28.6	1.5	$4.2\lambda_0\times 4.2\lambda_0$	4	8.6	23.31	0.002, NA	NA	Rogers RT 5880	NO	NO
[16]	28	26–29.5	3.5	$7\lambda_0\times10.26\lambda_0$	4	9.53	22	0.005, 9.75	73	Rogers R04350B	NO	NO
[17]	28	27.5–31	3.5	$12.6\lambda_0\times 7\lambda_0$	2	10	20	0.015, 9.99	NA	Rogers RT5880	NO	NO
[18]	28	25.5–32.5	7	$3.73\lambda_0\times 3.73\lambda_0$	4	5	25	0.12, 9.997	NA	FR4	NO	NO
Proposed	28	25.905–30.544	4.64	$2.24\lambda_0\times 2.24\lambda_0$	4	10.34	>26.065	0.0005, 9.99	98.35	Rogers RT 5880	YES	YES

symmetrical, so the first and second slots and the third and fourth slots share the same dimension. The antenna has a whole ground.

We are able to examine the front and rear sides of the proposed single-element antenna's precise geometry by referring to Fig. 2(a) and Fig. 2(b), respectively.

2.1.1. Parametric study

2.1.1.1. Effect of changing inset length (il). Fig. 3 shows the effect of changing the length of the inset. For values less than 0.5 mm, the resonant frequency is 27.456 GHz. At this point, the return loss is −17.794 dB, which is poor. If we increase the inset length more than our proposed value, in this case, 0.94 mm, the return loss decreases a bit, which is −24.409 dB, and the antenna resonates at 28.105 GHz.

So, decrementing the inset length causes us both frequency shift and more return loss, and incrementing the value of inset length causes comparatively less return loss but not as near as our proposed value.

2.1.1.2. Effect of changing length of substrate (sl). Fig. 4 shows us how crucial the length of the substrate is, for a lower value than the proposed value causes a poor return loss, which is −17.603 dB. But the resonant frequency remains almost at 28 GHz, more specifically, 28.083 GHz. If we increase the value of substrate length more than our proposed value, the return loss decreases, and it becomes −34.995 dB. But the resonance frequency shifts toward the right, which is 29.997 GHz, which is far from our desired value.

2.1.1.3. Effect of changing length of patch (pl). Fig. 5 shows us the importance of patch length. With a higher value than our proposed value, the reflection coefficient curve shifts left, and for a lower value than our proposed value, the reflection coefficient curve moves right. For 2.9 mm patch length, the resonance frequency is at 29.282 GHz, with a return loss of −21.197 dB. However, for 3.5 mm patch length, the resonant point is at 25.63 GHz, and return loss is −34.765 dB. It makes our design very flexible and gives us the option to manipulate the result.

2.2. Antenna array elements

The complete architecture of our 1×2 array antenna is depicted in Fig. 6. The two antenna elements relate to two feedlines having an impedance of 100 ohms and dimensions of Wf3×Lf3. A horizontal feed connects them with an impedance of 70.71 ohms and dimensions of Ws2×Ls2. Ultimately, the entire antenna is fed by a third feedline with an impedance of 50 ohms and dimensions of Wf1×Lf1, which extends from the center of the second feedline to the border of the board. This feedline serves as the primary connection and will be attached to the port. The array has a 3.6 mm edge-to-edge distance, which Dp-p denotes. The entire structure is engraved on the substrate with dimensions of Wa×La. Fig. 7 shows a comparison between the Reflection Coefficient

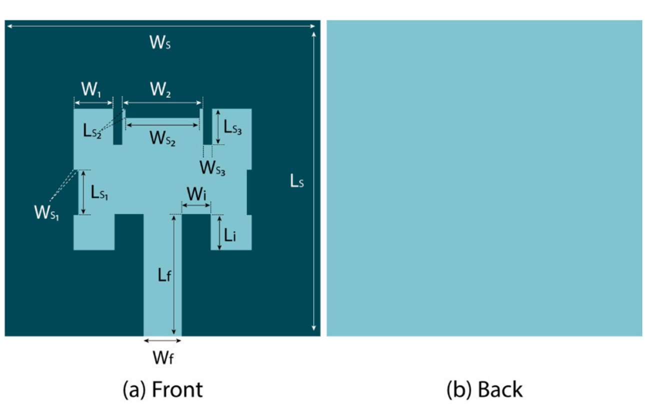

Fig. 2. Front and back view of single-element antennas.

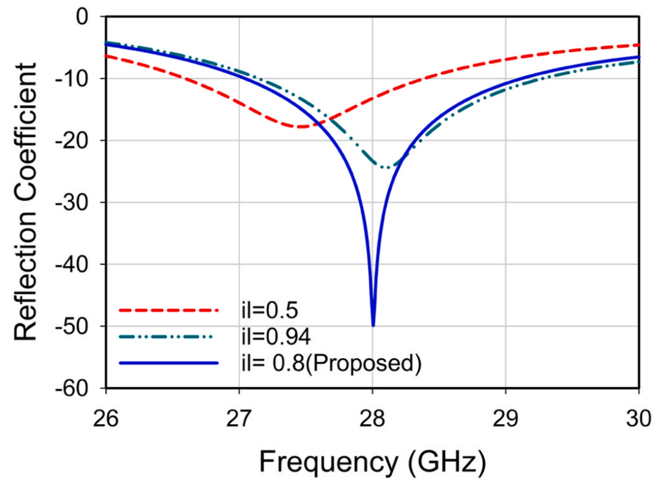

Fig. 3. Reflection Coefficient curve for various Inset Length (il).

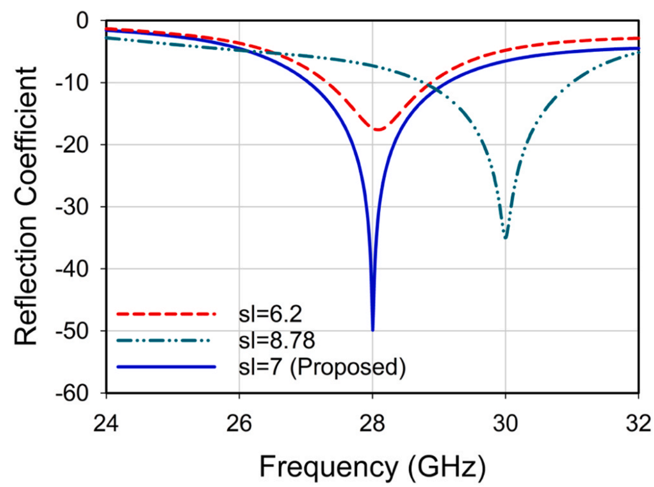

Fig. 4. Reflection Coefficient curve for various Substrate Length (sl).

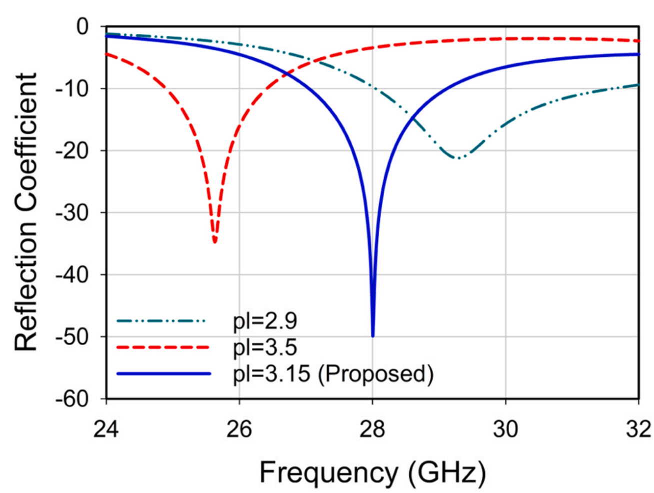

Fig. 5. Reflection coefficient curve for various patch length (pl).

curves of a single-element antenna and an Array element antenna. While the return loss and resonant frequency exhibit a close similarity, there is a distinct disparity in terms of bandwidth [20]. Fig. 8 compares the Gain and efficiency between individual elements and an array of elements.

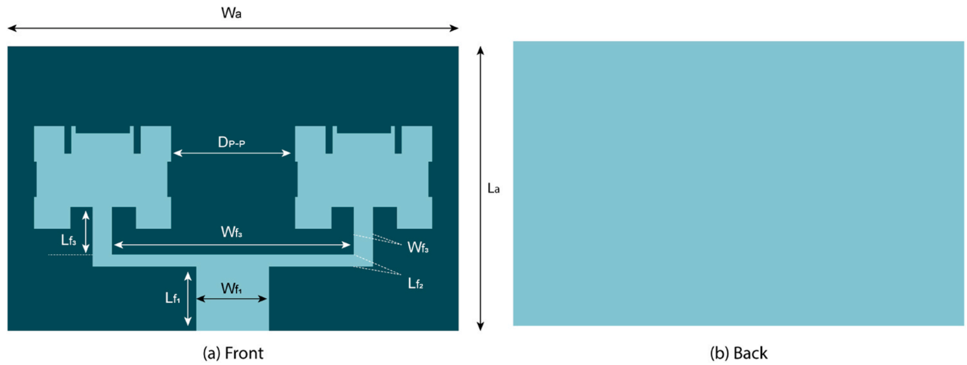

Fig. 6. Front and back view of array antenna.

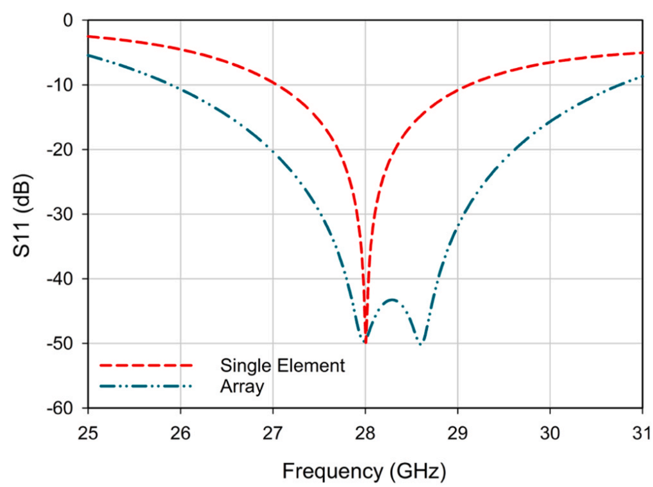

Fig. 7. Reflection coefficient of single element and array.

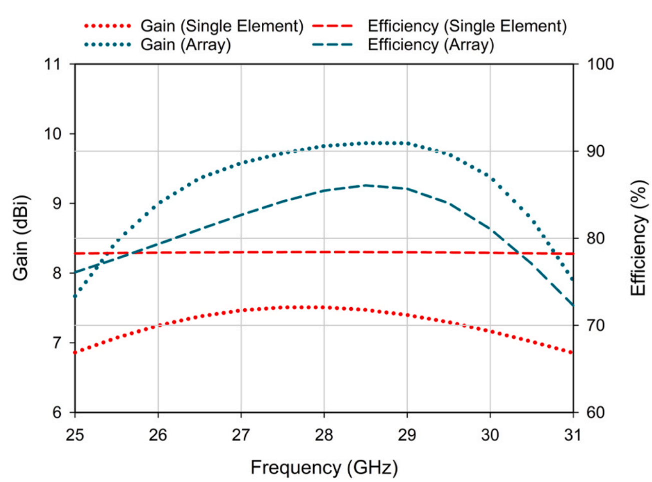

Fig. 8. Gain and efficiency of single element and array antenna.

The rise in Gain and efficiency from a single element to MIMO has been previously discussed.

2.3. Four-port MIMO antenna design

Fig. 9 displays the detailed design of the proposed MIMO antenna that comprises four elements.: four array antennas that we have primarily designed. The dimensions of each of the four elements remain unchanged. The board now has a dimension of Wm×Lm, with the four antenna elements engraved on each of the four sides of the board. However, the antennas are not located at the center of the sides but instead 5 mm away from the center. The distance between the edges of the antennas is 5.2 mm, represented as De-e mm, while the distance between the faces of the antennas is 12 mm, represented as Dx mm.

In Fig. 10, we can see the MIMO antenna's computed 28 GHz surface current pattern [21]. As illustrated in Fig. 10 (a), the highest surface current is 187.958 A/m, and the only antenna with a surface current is Ant.1. There is no surface current produced by additional antennas when Antenna 2 is operating, and the peak surface current is 187.962 A/m. When Ant. 3 or Ant. 4 is turned on, the behavior shown in Fig. 10 (c) and Fig. 10 (d) remains same, with peak surface currents of 187.958 A/m for both antennas.

3. Result and discussions

3.1. Reflection and transmission coefficients

The fundamental component of this single-element design, rectangular-shaped antenna with slots. Subsequently, we implemented a 1×2 array to enhance the gain and efficiency. Ultimately, we have successfully implemented a 4-element MIMO system to optimize its performance further.

The intricate design process of this antenna at various design stages is outlined in Fig. 11:

Fig. 12 (a) and (b) display the Reflection Coefficient curve at various stages of the design. The bandwidth had a significant rise, going from 2.078 GHz to 4.855 GHz. The gain also saw an increase, rising from 7.48 dB to 9.86 dB. Additionally, the efficiency improved from 78.17 % to 86 % when transitioning from a single element to an array. The gain in MIMO has further risen to a value of 10.34 dB. The reflection coefficient curve exhibits minimal variation between the array and MIMO configurations.

When designing a microstrip patch antenna, one of the crucial metrics that engineers consider is the reflection coefficient. This coefficient measures how well the antenna's feeding network or transmission line matches the antenna itself [22]. By optimizing this metric, engineers can maximize power transfer and reduce signal reflections to the source, which is essential for ensuring optimal antenna performance. In Fig. 13, we can see that the microstrip patch antenna under consideration exhibits a return loss of −49.476 dB at the resonance frequency of 27.86 GHz. The resonance occurs within a frequency range of 25.905 GHz to 30.544 GHz, offering a bandwidth of 4.64 GHz. Interestingly, there is a small peak at 28.63 GHz, with a return loss of −44.207 dB. This peak is significant in optimizing the antenna's performance. It is also worth noting that the measured result of our MIMO antenna is almost similar to that of the simulated MIMO antenna. We can see the prototype of our MIMO antenna in Fig. 15, and the result is shown in Fig. 16. Another critical metric that engineers consider when designing an antenna is isolation, which measures the impact of an

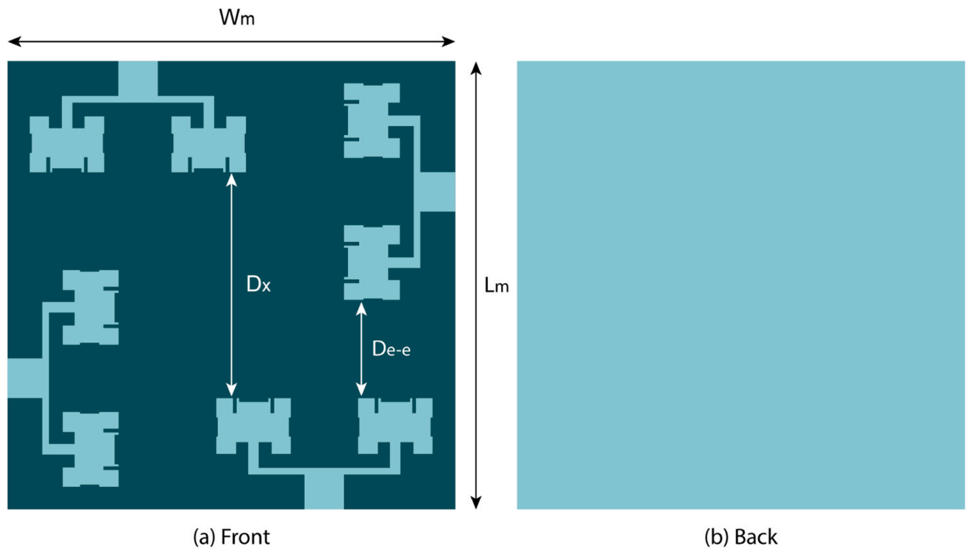

Fig. 9. Front and back view of proposed MIMO antenna.

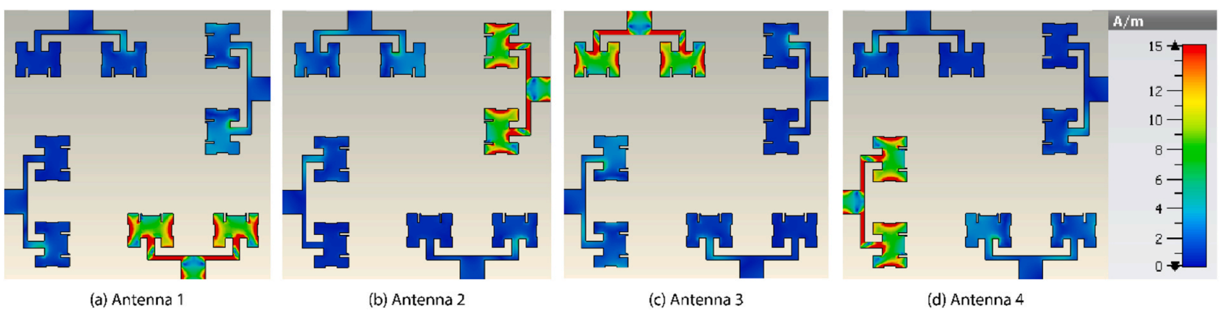

Fig. 10. Current distribution of proposed MIMO antenna.

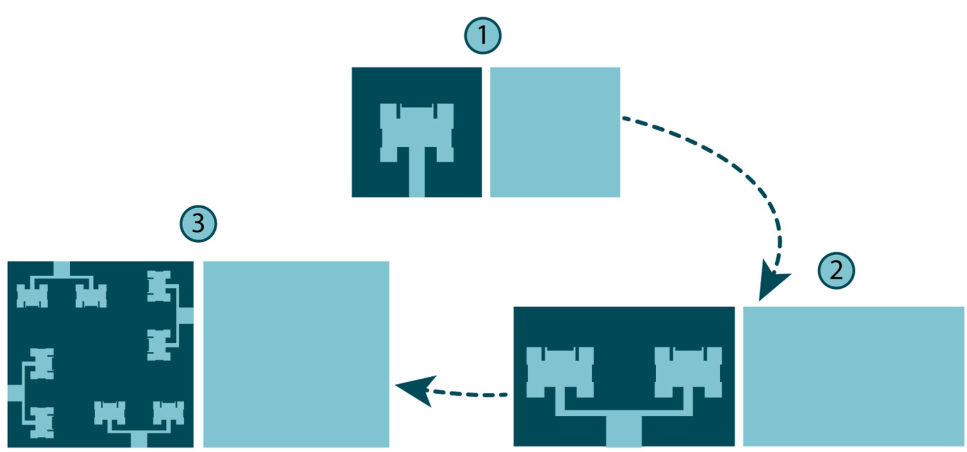

Fig. 11. Overall design of the proposed antenna (1) Single element, (2) Array, and (3) MIMO Antenna proposed.

antenna's radiation on other nearby antennas. Greater isolation suggests less interference between the antennas, leading to better overall performance. As shown in Fig. 14, the minimum isolation level between four antennas is 26.065 dB, achieved between pairs 1 and 2, 1 and 4, 2 and 3, and 3 and 4. Any isolation levels lower than this may indicate that the antennas are more susceptible to interference. Lastly, it is worth mentioning that the measured isolation is impressive, with around 25.93 dB, which almost touches the simulated result. Overall, the microstrip patch antenna's reflection coefficient and isolation are optimized for better performance, making it an excellent choice for various applications.

3.2. Gain and efficiency

Gain indicates how well an antenna concentrates energy in a specific direction. Communication range is proportional to antenna gain [23]. Applications prioritizing signal coverage require higher-strength antennas to communicate over longer distances. Gain also improves signal-to-noise ratio, making communication more transparent and more trustworthy. Efficiency refers to the extent of the antenna's

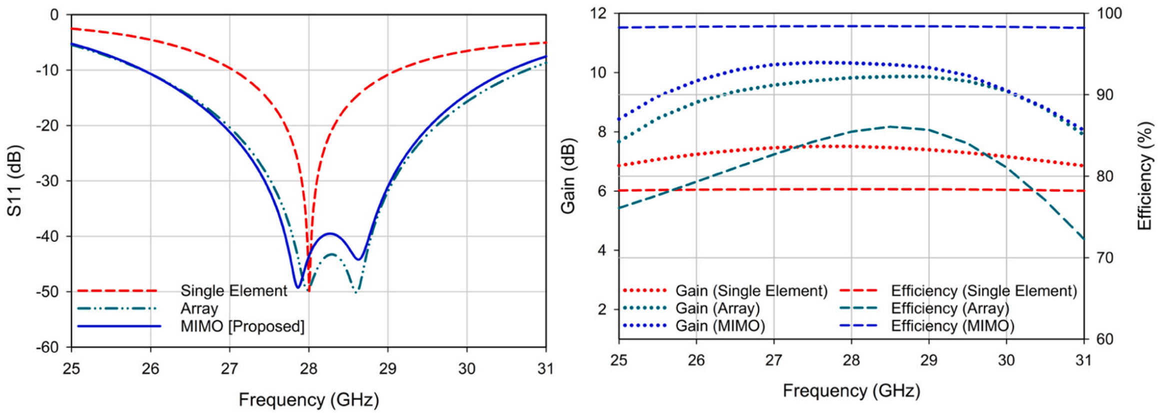

Fig. 12. (a) Reflection Coefficient (b) Gain and Efficiency of Each Step of the Antenna.

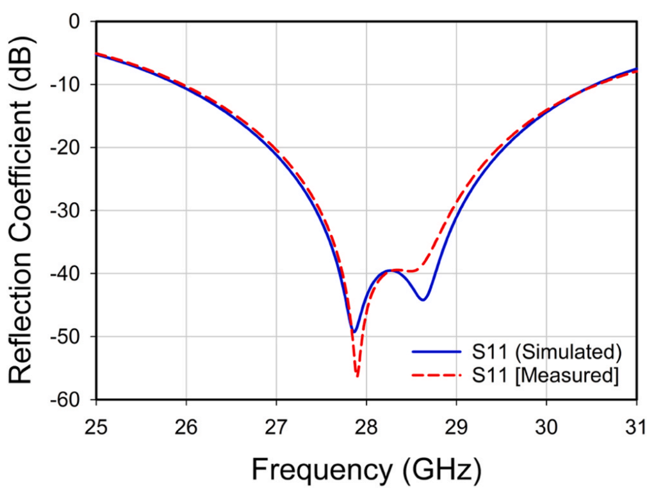

Fig. 13. Reflection coefficient of proposed MIMO antenna.

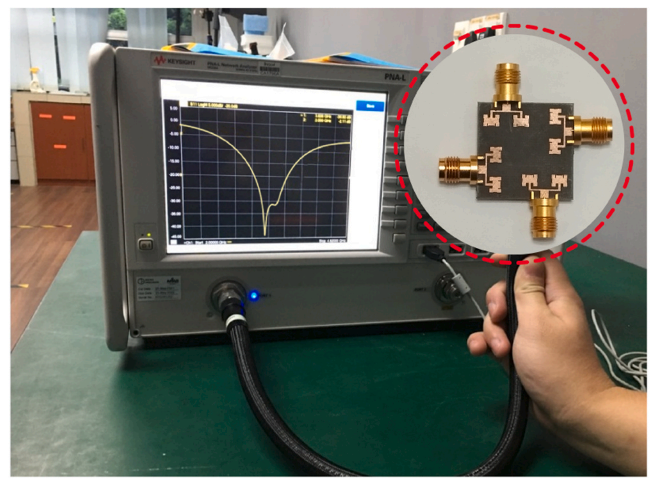

Fig. 15. Return loss measurement using vector network analyzer.

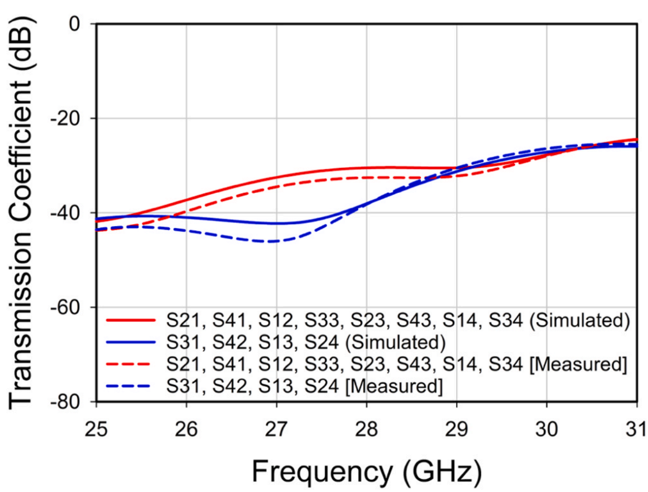

Fig. 14. Mutual coupling of proposed MIMO antenna.

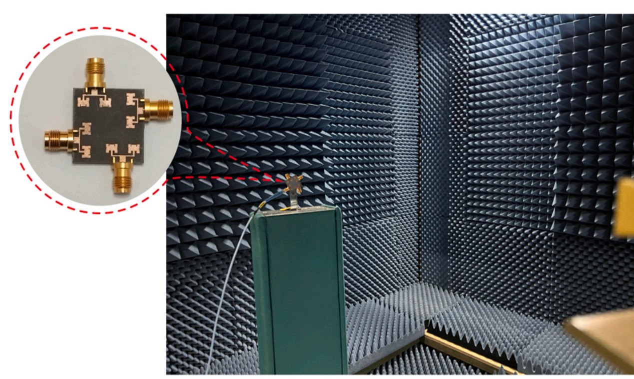

Fig. 16. Radiation characteristics measurement within an anechoic chamber.

power-to-radiation conversion. High-efficiency antennas reduce power losses and emit more input power as a usable signal. In accordance with Fig. 17, the antenna exhibits a peak gain of 10.34 dB, indicating exceptional performance. Additionally, the antenna demonstrates a maximum efficiency of 98.35 %, which underscores its impressive capabilities. Upon analyzing the data, we can observe that the measured gain and efficiency, are in line with the simulated results. However, upon closer inspection, we notice a slight deviation between the two parameters. While the measured gain is relatively consistent with the simulated outcome, the efficiency has slightly decreased and is now hovering around 97.5 %.

3.3. *Analysis of the proposed MIMO antenna's diversity performance*

In order to verify the effectiveness of the MIMO antenna system, it is imperative to examine specific attributes, commonly known as "MIMO performance metrics." The computation of these metrics can be obtained

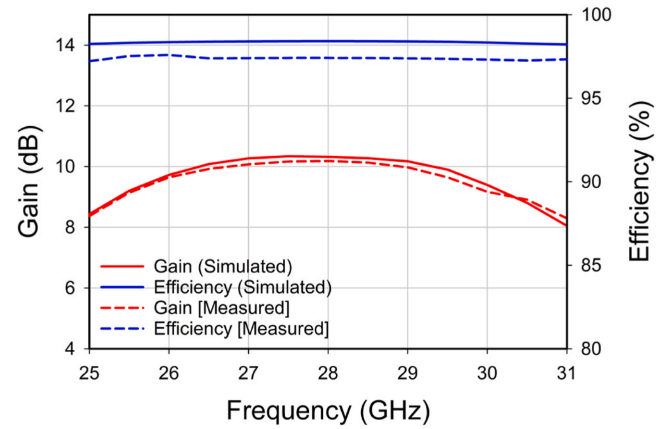

Fig. 17. Gain and efficiency of proposed MIMO antenna.

from the S-Parameters, which provide valuable insights into how mutual coupling and antenna impedance matching affect the diversity performance of the MIMO antenna.

3.3.1. The envelope correlation coefficient (ECC)

The ECC, computed by Eq. 1, is an essential metric employed to evaluate the likeness of radiation patterns generated by different antennas.

$$ECC = \frac{\left|\int_{4\pi}[E_1(\theta,\varphi) * E_2(\theta,\varphi)]d\Omega\right|^2}{\int_{4\pi}|E_1(\theta,\varphi)|^2 d\Omega \int_{4\pi}|E_2(\theta,\varphi)|^2 d\Omega} \quad (1)$$

Where, E_1 (θ,ϕ) and E_2 (θ,ϕ) are the complex electric field patterns of the two antennas.

Ω represents the solid angle over a sphere, encompassing θ (the elevation angle) and ϕ (the azimuth angle).

dΩ represents the differential element of the solid angle.

The integrals are performed over the entire sphere, denoted by 4π.

The computed ECC value is less than 0.0012, as depicted in Fig. 18. The optimal value for the ECC of an uncorrelated MIMO antenna is zero. Nevertheless, in practical MIMO settings, it is imperative to maintain the (ECC) at a maximum value of 0.5 throughout the whole proper frequency spectrum [24]. Based on the data we have collected; it appears that the measured error correction code (ECC) matches the simulated result. However, we have also observed some changes that are visible in the region outside of our bandwidth, as depicted in Fig. 18.

3.3.2. Diversity gain(DG)

Diversity Gain is an essential attribute that seeks to enhance the quality and dependability of a signal by employing many signal paths that are independent of each other. It is linked to ECC. As the Envelope Correlation Coefficient lowers, the value of DG increases. The maximum value of DG is measured at 10 decibels. The following equation can compute the value of DG in a MIMO system [25].

$$DG = 10\sqrt{1 - ECC^2} \quad (2)$$

The graph depicted in Fig. 19 illustrates the DG value for the proposed MIMO system. The data indicates that the lowest DG value observed is 9.99 dB, which signifies outstanding performance in antenna diversity. Upon analyzing the DG measurement result, we have come to the realization that it remains consistent with the simulated result. Upon closer inspection, we haven't found any noteworthy changes in the result within the bandwidth, as displayed in Fig. 19. It can be inferred that the DG measurement result is reliable and can be considered accurate based on consistency in comparison with the simulated result.

3.3.3. Channel capacity loss (CCL)

The Channel Capacity Loss (CCL) is a crucial statistic employed to evaluate the efficiency of MIMO Antennas. The ability to transmit information or signals via a channel without any interruptions is assessed by measuring the Channel Capacity Limit (CCL). As the number of antenna elements in a MIMO system increases, the channel capacity also increases in direct proportion. Capacity losses occur due to the correlation between the MIMO channels. The CCL, or Channel Capacity Loss, is an essential measure for quantifying the MIMO channel capacity when there is a correlation. It may be calculated using Eq. 3 [26].

$$CCL = -\log_2 \det(p_R). \quad (3)$$

Eq. 4 can be utilized to calculate the two-port correlation matrix at the receiver.

$$p_R = \begin{pmatrix} \&\rho_{xx} & \rho_{xy} \\ \&\rho_{yx} & \rho_{yy} \end{pmatrix} \quad (4)$$

Where,

$$\&$$
$$\rho_{xx} = 1 - \left(|S_{xx}|^2 + |S_{xy}|^2\right).$$
$$\&\rho_{yy} = 1 - \left(|S_{yy}|^2 + |S_{yx}|^2\right).$$
$$\&\rho_{xy} = \left|S_{xx}^* S_{xy} + S_{yx}^* S_{xy}\right|^2.$$
$$\&\rho_{yx} = \left|S_{yy}^* S_{yx} + S_{xy}^* S_{yx}\right|^2.$$

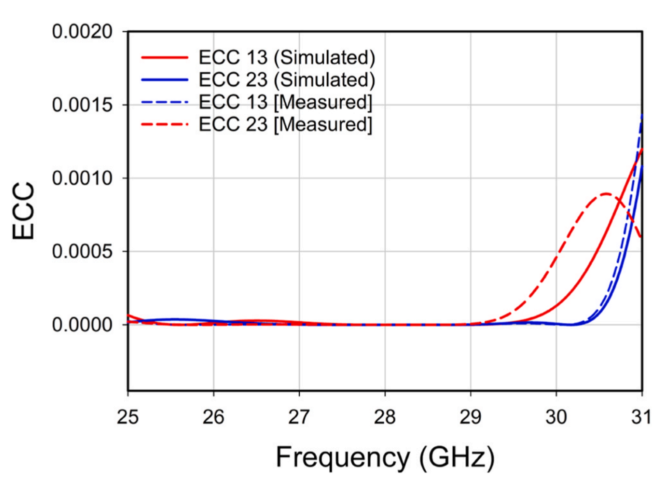

Fig. 18. ECC of proposed MIMO antenna.

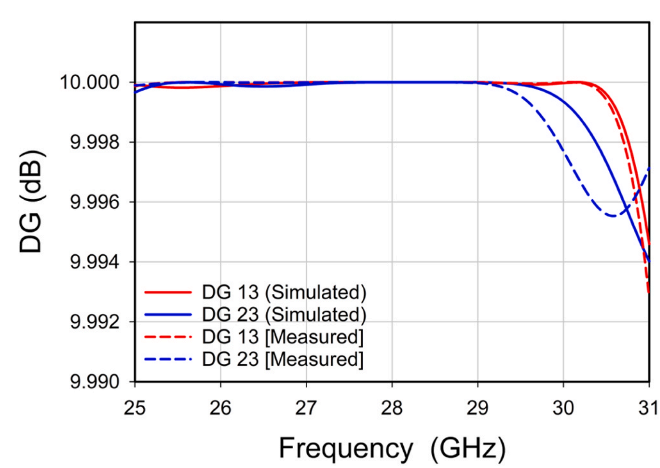

Fig. 19. DG of proposed MIMO antenna.

The coefficients for ports 1 and 2 are denoted as (x) and (y), respectively. The suggested value for the CCL standard is less than 0.5 bps/Hz. Fig. 20 illustrates the recommended antenna's Channel Capacity Loss (CCL). A CCL of less than 0.4 bps/Hz is generally desirable [27]. The Channel Capacity Loss (CCL) for the proposed antenna is consistently less than 0.15 bits per second per Hertz (bps/Hz) throughout the whole operational frequency range.

3.3.4. Total active reflection coefficient (TARC)

TARC, which stands for Total Active Reflection Coefficient, is a critical metric in four-port antennas since it provides insight into the correlation between transmitted and received power. Eq. 5 can be utilised to ascertain this [28].

$$TARC = \frac{\sqrt{\left(|S_{xx}| + |S_{xy}|\right)^2 + \left(|S_{yx}| + |S_{yy}|\right)^2}}{\sqrt{4}}. \quad (5)$$

An ideal Total Active Reflection Coefficient (TARC) for a Multiple-Input Multiple-Output (MIMO) antenna would be <0 dB. The simulated outputs of TARC for the proposed antenna are displayed as <-10 dB, in Fig. 21.

3.3.5. Mean effective gain (MEG)

The radiated power level from the two antenna elements must be kept at a virtually zero difference. The quantification of this distinction can be determined by comparing the power ratio between two antennas, which is derived using the Mean Effective Gain of both antenna elements.

$$k = \min\left(\frac{MEG_1}{MEG_2}, \frac{MEG_2}{MEG_1}\right) \quad (6)$$

MEG_i is the average effective gain of the antenna element being discussed. The MEG for both antenna elements and power ratio (k) is displayed in Fig. 22. The Mean Effective Gain for an N Port MIMO Antenna can be mathematically represented as [29].

$$MEG_i = 0.5\left[1 - \sum_{j=1}^{N} S_{ij}\right] \quad (7)$$

Based on Fig. 22 data, the MEGs of the two antenna elements fluctuate between −7.8 dB to −4.5 dB across the entire frequency spectrum. This range is more suitable for MIMO performance. The standard variation range of $-12.0dB \leq MEG_i \leq -3dB$ is recommended for MIMO systems to achieve optimal performance. The variation of MEGs, represented by the k =power ratio, ranging from 0 dB to 0.3 dB within the band. Therefore, the significant similarity between the MEGs of the antenna elements results in a strong diversity performance.

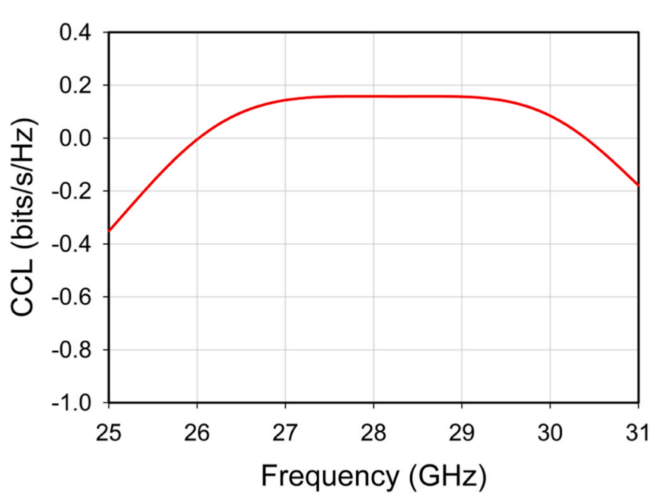

Fig. 20. CCL of proposed MIMO antenna.

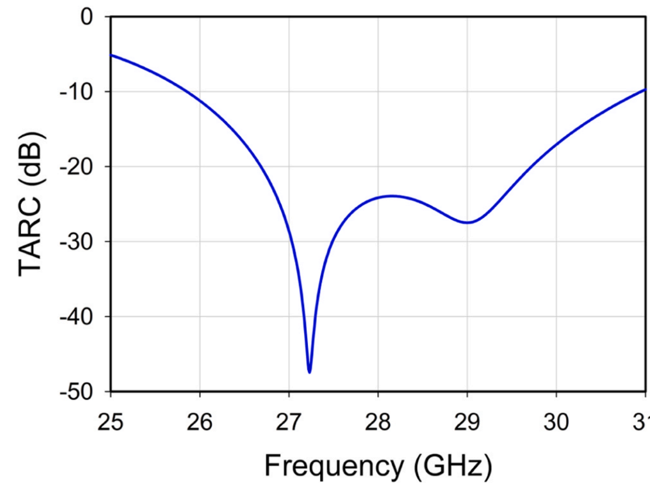

Fig. 21. TARC of Proposed MIMO Antenna.

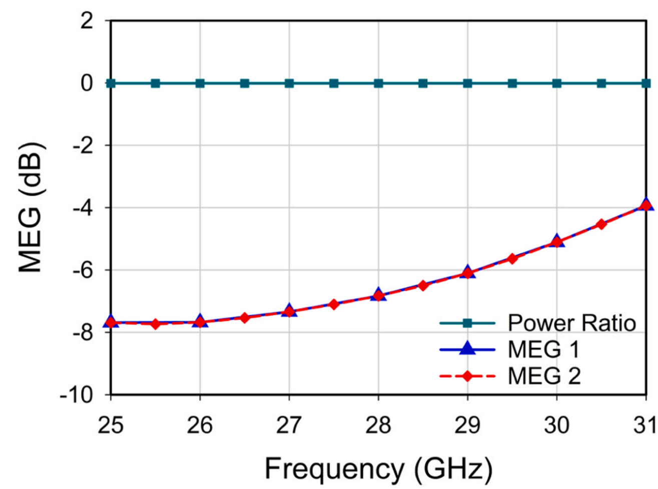

Fig. 22. MEG of proposed MIMO antenna.

3.4. Radiation pattern

The radiation pattern depicts the three-dimensional emission and absorption patterns of electromagnetic waves as they travel through an antenna [30]. It demonstrates the variation in radiated power as a function of beam direction. The letters "XY," "YZ," and "ZX" indicate the antenna orientations and the corresponding planes on which the radiation pattern is observed when describing the pattern on different planes [31]. An antenna's electric field can be seen in its E-field radiation pattern, which plots the field's direction and strength against the antenna's azimuthal angle (phi). The patterns of emission from an antenna's magnetic field (H-field) provide light on why the strength and direction of the field change as a function of the polar angle (theta). The lobe magnitude at ϕ= 90° is 23.3 dB V/m, the half-power beam width is 27.5°, and the primary lobe magnitude of the E-field is 3 dBV/m at ϕ= 0° at 28 GHz frequency, all at an angular beam width of 36.6 degrees at 3 dB. At theta= 90 degrees, the main lobe magnitude is −43.7 dB A/m, and the half-power beam width (HPBW) of the H-field is 26.7 degrees, as shown in Fig. 23. In Fig. 23, the radiation pattern that has been measured is quite remarkable since it closely resembles the simulated result. This indicates that the simulation has been successful in replicating the real-world scenario with a high degree of accuracy. The similarity between the measured and simulated radiation patterns is

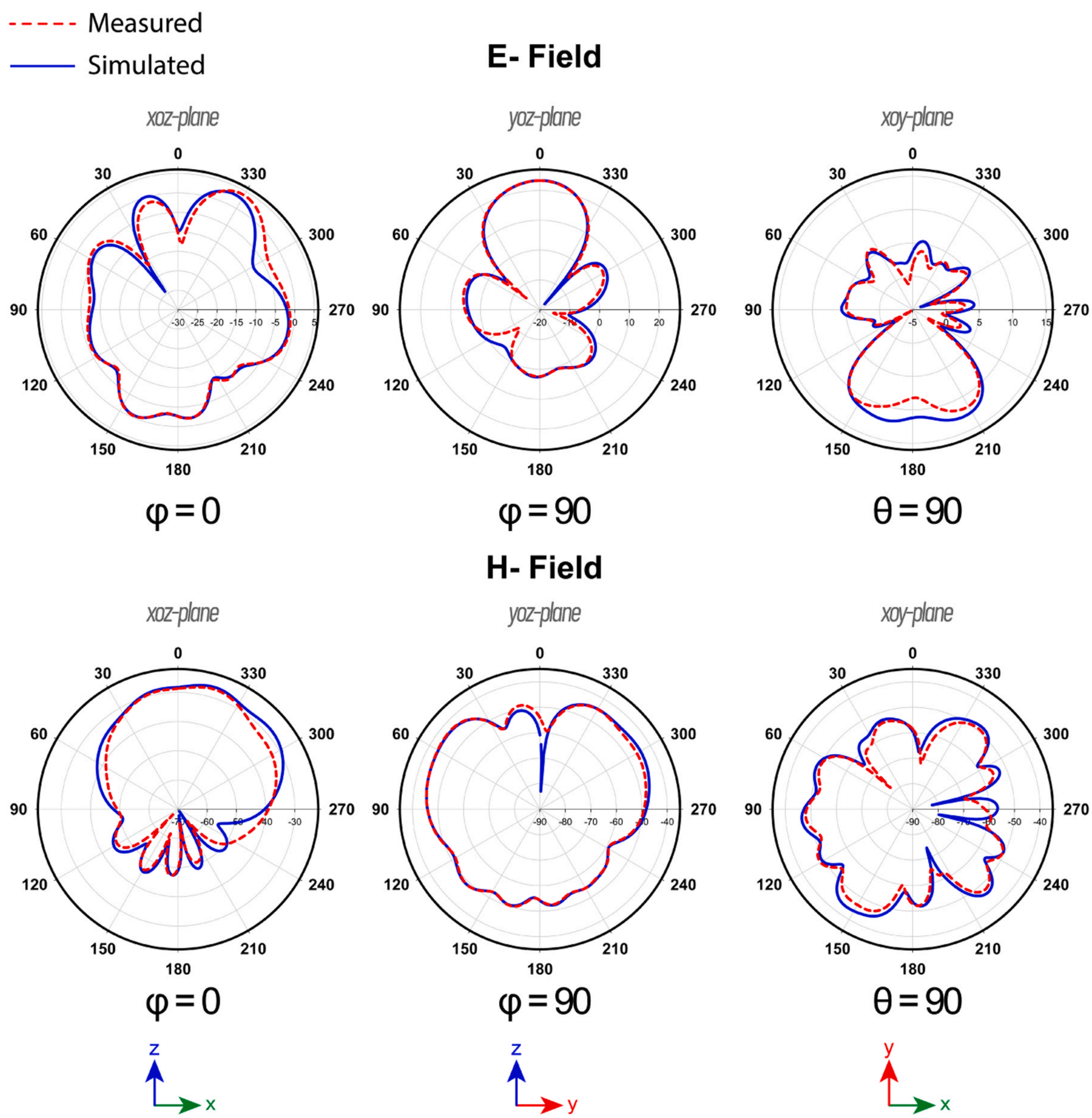

Fig. 23. Radiation pattern of Proposed MIMO antenna at 28 GHz.

indeed impressive and points towards the effectiveness of the simulation process.

4. RLC equivalent circuit

In order to calculate the RLC (resistance, inductance, and capacitance) parameters for the antenna array and MIMO (multiple-input, multiple-output) antenna circuits shown in Fig. 24 and Fig. 25, it is recommended to use the impedance analysis tools provided by CST Studio. CST Studio is a comprehensive simulation and circuit design platform that is bundled with Agilent ADS, a widely-used software for electronic design automation. The components L1, C1, and R1 dictate the initial resonant frequency, while L2, C2, and R2 define the subsequent resonant frequency. The spacing between the array elements is associated with positions Lp-p and Cp-p, whereas the 100-ohm feed is associated with positions Lf1 and Cf1. Lf2L and Cf2L handle the 70-ohm feed of the left half of the circuit, while Lf2R and Cf2R handle the 70-ohm feed of the right half. The components L1–2 and C1–2 are responsible for the inductance and capacitance between antenna 1 and antenna 2, while C2–3 and L2–3 are responsible for antenna 2 and antenna 3.

Similarly, C3–4 and L3–4 are responsible for the inductance and capacitance between antenna 3 and antenna 4, and C1–4 and L1–4 are responsible for antenna 1 and antenna 4. Components C2–4 and L2–4 are shared between antenna 2 and antenna 4. Components C1–3 and L1–3 account for the inductance and capacitance between antenna 1 and antenna 3. Table 2 presents a list of the values of the circuit elements used in the MIMO antenna. This table can be used as a reference to estimate the antenna's performance. Additionally, Fig. 26 provides a comparison of the results obtained from the CST simulation and a circuit simulation that utilizes the S11 parameters. This comparison can help to evaluate the accuracy of the circuit model and the antenna's effectiveness.

5. Machine learning analysis

Machine learning-assisted optimization involves the application of machine learning (ML) methods to improve and streamline the optimization process across many areas. The utilization of machine learning techniques can be advantageous in the process of determining the most

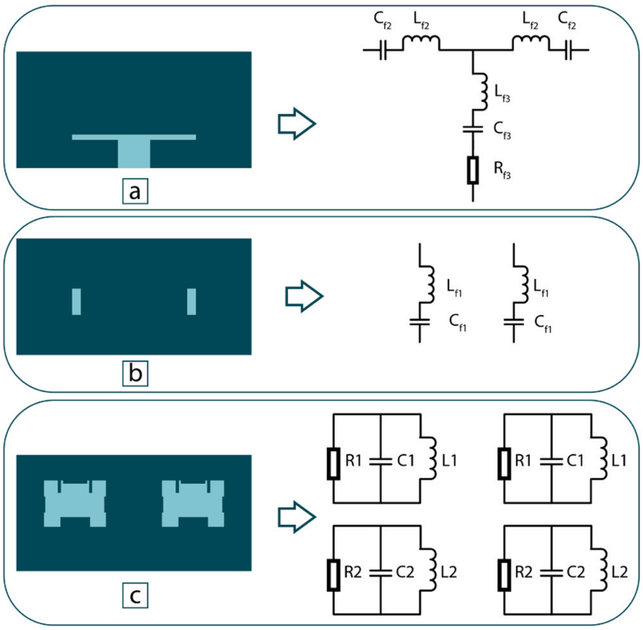

Fig. 24. Equivalent circuit of the array antenna.

suitable optimization algorithm for a specific problem. Through the examination of the attributes of the optimization problem, machine learning models possess the capability to suggest or autonomously select the method that is anticipated to exhibit superior performance [32]. The application of machine learning techniques to optimization can yield enhancements in efficiency, accuracy, and adaptability while dealing with intricate and ever-changing situations. This phenomenon arises because of the distinctive operational mechanisms of antennas [33]. The utilization of machine learning techniques has significant importance in the context of this inquiry.

The technique can be divided into two primary components, both of which are described below. The first thing that must be done is to make the MIMO antenna in CST, which is a simulation tool. After that, the dataset that was generated through a parametric sweep needs to be extracted, as depicted in Fig. 27. At this point, the first stage will be finished. During the process of examining the dataset, a machine learning model needs to be trained so that it can determine which approach yields the best outcomes. To estimate the gain of the suggested antenna, we first simulate it with CST Microwave Studio (MWS), then accumulate 120 data points, and finally estimate it using a variety of regression machine learning techniques.

There are one hundred different data points that need to be investigated. The training consisted of 80 samples, whereas the validation consisted of 20 samples. Additionally, the thickness of the patch has the greatest influence on the key outputs of our dataset, which is the gain. This is demonstrated in Fig. 28 which demonstrates that the length, width, and height of the substrate have the greatest impact. The training dataset is subsequently processed by a machine learning method after the collection of features and labels has been completed. After being trained and verified, a model has the potential to produce accurate predictions of several outputs based on a range of inputs, including gain. These predictions can be of a high degree of accuracy.

5.1. Regression machine learning model analysis

Supervised regression models are a subset of machine learning models that use labeled datasets to make predictions about continuous target variables. Regression assignments aim to teach mapping from input features to a continuous output. Determining the strengths and limitations of a regression machine learning model, as well as its performance, and learning about the connections between input data and the target variable are all part of the analysis process. Sort the data into two sets: one for training purposes and another for testing. A model is trained using the training set, and its performance on unseen data is evaluated using the testing set. Bring the model's hyperparameters up to optimum performance [34].

5.1.1. Decision tree regression

One supervised machine learning tactic that can be hired for the prediction of continuous numerical values is Decision Tree Regression. With the help of some splitting criteria, we can construct a tree structure where each leaf node stands for a predicted value of the target variable. Making forecasts requires building the tree from the ground up and then climbing all the way to the leaf node. At each leaf node, the matching input is given the anticipated value [35].

5.1.2. Random forest regression

Using a Random Forest as a regression model the regressors in a regression model are a group of decision trees. The Random Forest makes its final prediction by averaging the projections from all the trees. A typical way to aggregate results from regression is to average the predictions [36].

5.1.3. Nonparametric regression

Nonparametric regression is a valuable tool in cases where a basic parametric model fails to adequately capture the underlying relationship. Cross-validation slants, such as leave-one-out cross-validation or k-fold cross-validation, are frequently employed in evaluating the efficacy of various models and determining the optimal fit for the given data [37].

5.1.4. Extreme gradient boosting (XGB) regression

XGBoost has gained significant popularity in diverse machine-learning contests and real-world applications because to its exceptional performance, scalability, and adaptability. XGBoost is a software library that serves as an implementation of gradient boosting, a popular ensemble learning technique. Ensemble learning is a technique that aims to enhance overall performance by aggregating the predictions of different models [38].

5.1.5. Gaussian process regression

The Gaussian Process regression's predictive distribution offers both the mean forecast and the accompanying uncertainty of the prediction. The representation of this uncertainty is denoted by the variance of the predictive distribution. It is possible to generate predictions for a given set of input points, and the model inherently accounts for the uncertainty in areas with sparse data.[39]

5.1.6. Random sample consensus (RANSAC) regression

A robust method for estimating model parameters from a set of data points that may include outliers is RANSAC, an iterative algorithm. In computer vision, picture analysis, and robust regression applications, RANSAC is frequently used. Where there is a high likelihood that outliers may skew the results, RANSAC is a useful tool for fitting regression models to the data [40].

5.2. Performance measurement metrics

A regression model's accuracy in predicting the target variable can be measured using several different metrics. Evaluating the model on several metrics allows us to optimize performance, fine-tune it, and accept a better outcome, which is essential for building and deploying a generalized model [41]. Visualizing the predicted values vs, the actual values in the holdout set is the optimal slant to examine regression data. Our statistical measures for evaluating these models include R-squared (R2), Explained Variance Score (Var Score), Mean Squared Error (MSE),

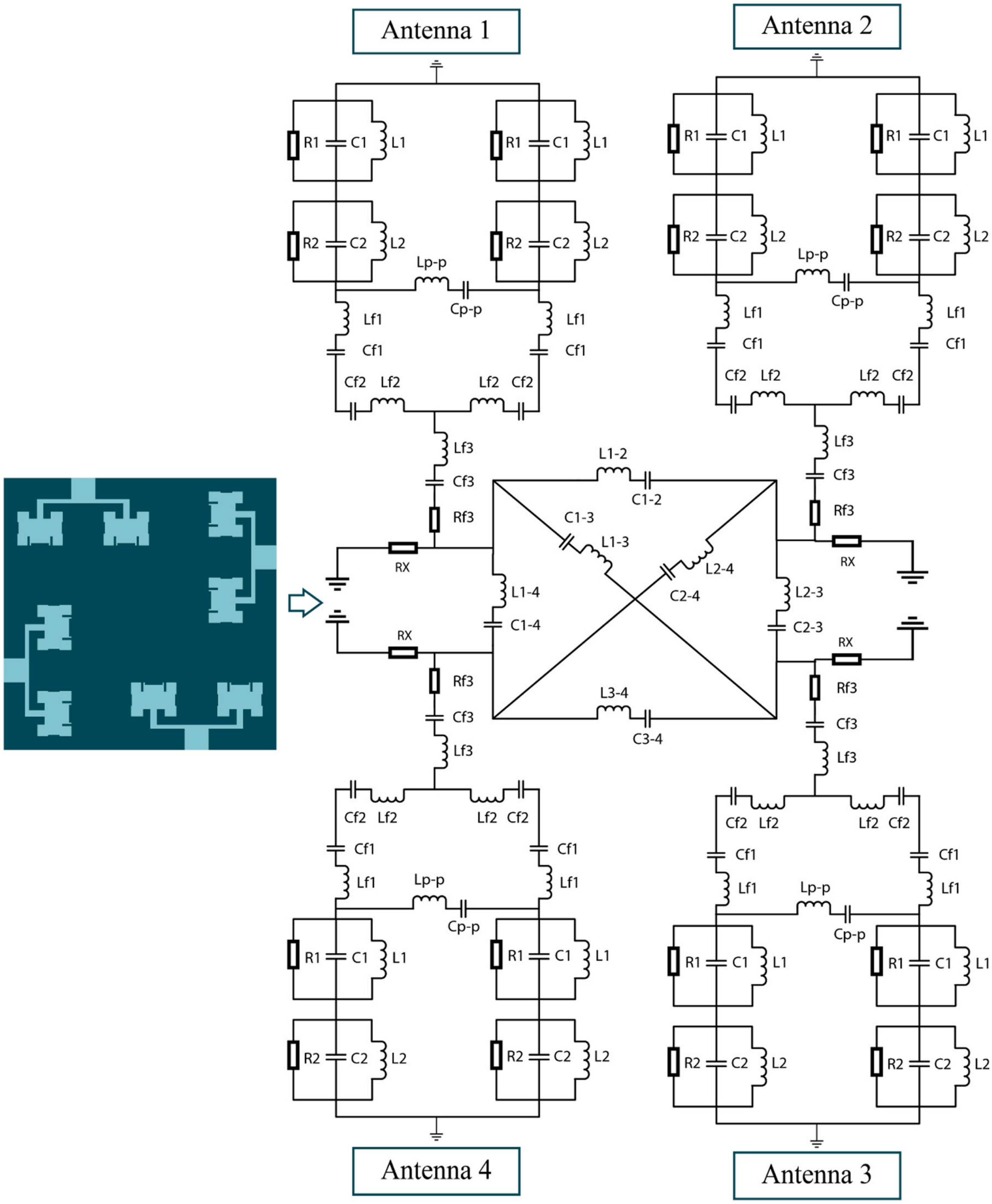

Fig. 25. Equivalent circuit of proposed MIMO antenna.

Root Mean Squared Error (RMSE), and Mean Absolute Error (MAE) [42].

The Mean Absolute Error (MAE) is calculated by taking the complete difference between the expected and actual values and averaging them [43]. By utilizing the absolute difference, we can guarantee that over-estimations and underestimations contribute equally to the total error. Here is the given expression:

$$MAE = \frac{1}{n} \sum_{i=1}^{n} |y_i - \hat{y}_i| \tag{8}$$

Where, n = number of errors, y_i is the actual value, $\hat{y}_i$ is the predicted value, $|y_i - \hat{y}_i|$ = error absolute

The Mean Squared Error, often known as MSE, is a statistic that is frequently applied to evaluate the effectiveness of a regression model. The squared disparity between the genuine values and the expected values is what it represents. The squared method is utilized by us to prevent the cancellation of negative terms, which is a benefit enjoyed by MSE.

$$MSE = \frac{1}{n} \sum_{i=1}^{n} (y_i - \hat{y}_i)^2 \tag{9}$$

The Root Mean Squared Error (RMSE) is a well-known statistic that is applied commonly for the persistence of assessing the usefulness of a regression model. Mean squared error (RMSE) is a straightforward square root of mean squared error, as the name of the statistic itself

Table 2
Optimized antenna parameters.

Parameter	Value	Parameter	Value	Parameter	Value	Parameter	Value
Ws	7	Ls_2	0.2	Wa	13.14	Wf_3	0.6
Ls	7	Ws_3	0.2	La	8.3	Lf_3	1.5
W_1	0.88	Ls_3	0.8	Dp-p	3.6	Wm	24
W_2	1.6	Wi	0.65	Wf_1	2.15	Lm	24
Ws_1	0.1	Li	0.8	Lf_1	1.85	Dx	12.05
Ls_1	1	Lf	2.73	Wf_2	8.2	De-e	5.28
Ws_2	1.6	Wf	0.79	Lf_2	0.4	h	0.787

Here, Ws - Substrate width; h- Substrate height; Ls - Substrate width; W_1 - Width of slot 1; W_2 - Width of slot 2; Ws_1 - Width of slot 1; Ls_1 - Length of slot 1; Ws_2 - Width of slot 2; Ls_2 - Length of slot 2; Ws_3 - Width of slot 3; Ls_3 - Length of slot 3;Wi - Inset width; Li- Inset length; Lf- Feed length; Wf- Feed width; Wa - Width of array; La - Length of array; Dp-p - Distance from patch to patch; Wf_1 - Width of feed 1 (Array); Lf_1 - Length of feed 1 (Array); Wf_2 - Width of feed 2 (Array); Lf_2 - Length of feed 2 (Array); Wf_3 - Width of feed 3 (Array); Lf_3 - Width of feed 3 (Array); Wm - Width of MIMO; Lm - Length of MIMO; Dx - Distance from patch to patch in MIMO; De-e - Distance from edge to edge of patch in MIMO.

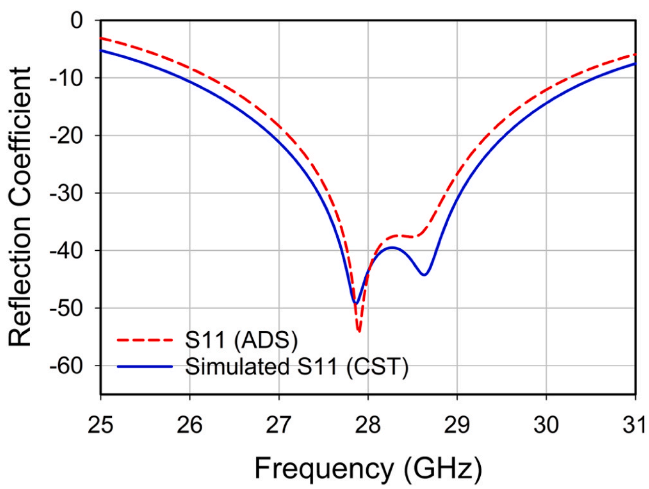

Fig. 26. Reflection coefficient of ADS and CST.

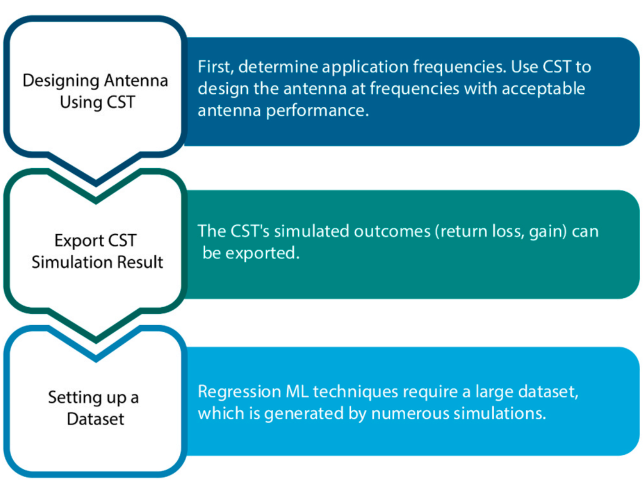

Fig. 27. Data acquisition workflow for Machine Learning.

makes it abundantly evident.

$$RMSE = \sqrt{\frac{1}{n} \quad \sum_{i=1}^{n} (y_i - \quad \widehat{y}_i)^2} \tag{10}$$

In a regression model, R-squared, which stands for "coefficient of determination," is a statistical portion that shows how much of the distinction in the dependent variable can be explained by the independent factors. Not the exact number of wells your model performed, but a measure of how well it did. This is called the R^2 score.

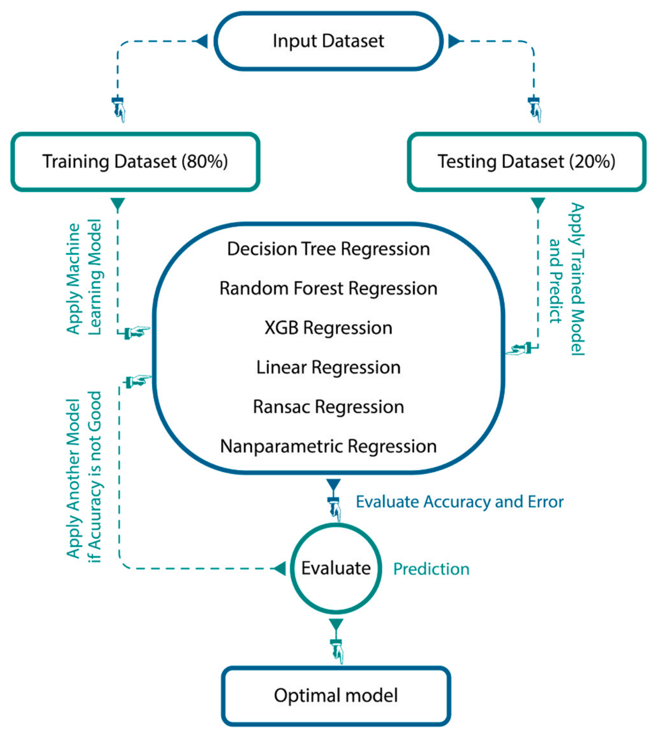

Fig. 28. Schematic depicting the steps required to develop machine learning.

$$R^2 = 1 - \frac{\sum_{i=1}^{N} (y_i - \widehat{y}_i)^2}{\sum_{i=1}^{N} (y_i - \widehat{y}_i)^2} \tag{11}$$

In regression models, the word "variance score" is commonly used to refer to the R-squared or coefficient of determination. The mode-dependent independent variables explain a certain percentage of the total distinction in the dependent variable, as measured by R-squared.

$$\text{explained variance}(y, \widehat{y}) = 1 - \frac{\text{Var}(y - \widehat{y})}{\text{Var}(y)} \tag{12}$$

Where, y is the actual value, $\widehat{y}$ is the predicted value, Var (y - $\widehat{y}$) is the variance of the prediction errors (residuals), Var (y) is the variance of the actual values.

5.3. Result analysis M/L

Table 3 provides a summary of the comparative advantages of various regression methodologies, including XGBoost (XGB), decision

Table 3
The gain prediction performance.

Algorithms	MAE	MSE	RMSE	R-Square	Var Score	MAPE
Decision tree regression	9.03 %	1.30 %	11.40 %	78.42 %	79.54 %	1.26 %
XGB Regressor	9.30 %	1.26 %	11.26 %	78.95 %	81.95 %	1.24 %
Gaussian Process Regression	0.36 %	0.00 %	0.63 %	97.97 %	98.05 %	0.08 %
Random Forest Regression	8.72 %	1.16 %	10.79 %	80.66 %	82.51 %	1.15 %
RANSAC Regression	8.65 %	11.55 %	10.75 %	80.82 %	82.19 %	1.16 %
Nonparametric Regression	9.52 %	1.32 %	11.53 %	77.95 %	81.65 %	1.26 %

tree, nonparametric, Gaussian process regression, RANSAC, and random forest. The accuracy of each method is assessed through the utilization of several metrics, including R-squared, variance score, mean squared error (MSE), mean root-mean-squared error (RMSE), and mean absolute error (MAE). Moreover, the utilization of Fig. 29 employs a bar chart to visually represent the comparative performance of these models. The findings indicate that the random forest regression model exhibits negligible discrepancies in terms of Mean Absolute Error (MAE) (0.36 %), Mean Squared Error (MSE) (0.40 %), Root Mean Squared Error (RMSE) (0.63 %), and Mean Absolute Percentage Error (MAPE) (0.90 %). The accuracy of the variance score is reported to be 98.05 %, while the R-squared value is found to be 97.97 % in the context of Gaussian process regression.

Gaussian process regression was used to run twenty test samples, and Fig. 27 demonstrates the predicted and simulated improvements for these samples. From 6.5 dB to 7.7 dB, we change the gain for the investigation. The results of the simulated and predicted gains for gaussian process regression show a minor variation, as shown in Table 4. Results from the simulation and the expected outcome are thus highly congruent, as seen in Fig. 30. This ML model, gaussian process regression, is chosen for its exceptional ability in forecasting future benefits.

6. Conclusion

In this work, a MIMO antenna design, modelling, dimension of the manufactured antenna model, equivalent RLC circuit analysis, and a variety of machine learning approaches are incorporated to evaluate the performance of the anticipated applications for 5 G. The proposed MIMO antenna was initially designed with the help of the CST simulation tool. It possesses a maximum gain of 10.34 dB, the highest isolation more significant than 26, and a maximum efficiency of 82.85 %. Furthermore, the RLC equivalent circuit model of the antenna built by ADS Agilent and the CST-simulated antenna design offer substantially equal performances. In addition, six different regression models have been utilized to ascertain the antenna's gain. When the results of the simulation and the anticipated results are compared, the data samples

Table 4
Simulated and predicted Gain comparison using Gaussian Process Regression.

No	Simulated Gain	Predicted Gain	No	Simulated Gain	Predicted Gain
1	7.685	7.677454	11	7.295	7.207454
2	7.474	7.504536	12	7.601	7.577454
3	7.699	7.677454	13	7.475	7.577454
4	7.385	7.477454	14	7.643	7.577454
5	7.529	7.577454	15	7.622	7.577454
6	7.644	7.577454	16	7.423	7.477454
7	7.659	7.677454	17	7.512	7.577454
8	7.554	7.577454	18	7.562	7.577454
9	7.471	7.577454	19	7.551	7.577454
10	6.559	6.460967	20	7.787	7.818481

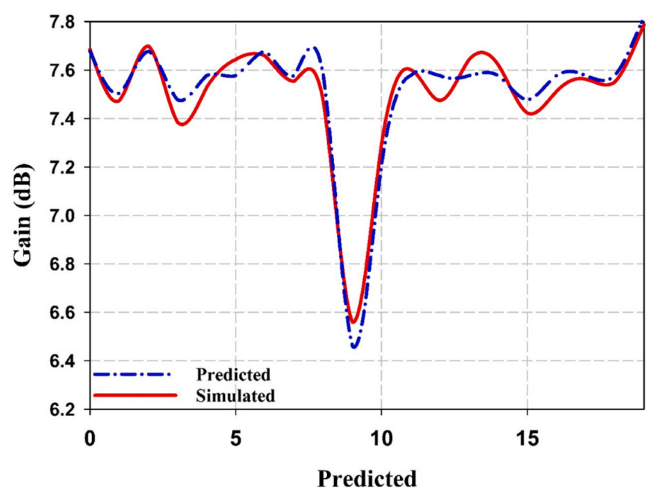

Fig. 30. Simulated vs. predicted gain using gaussian process Regression.

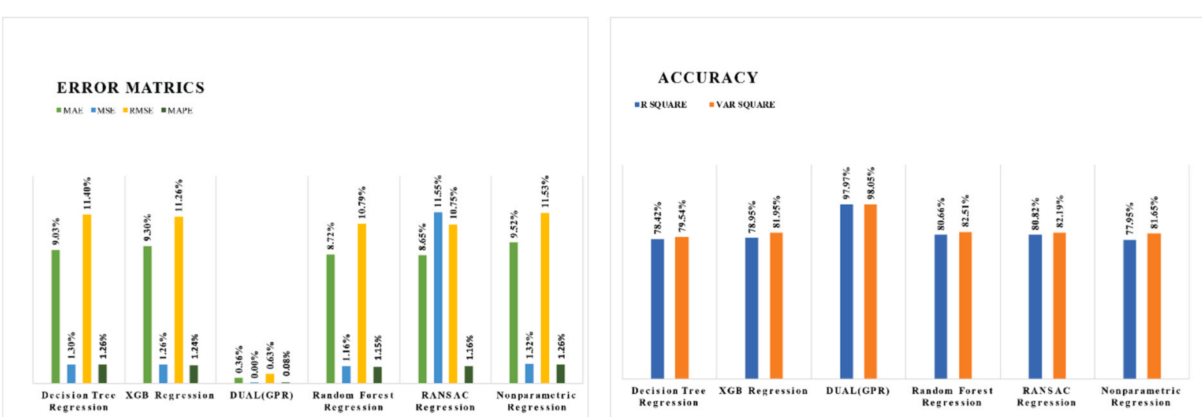

(a) Error metrics bar chart (b) Accuricy comparative bar chart

Fig. 29. Performance comparative bar chart.

are startlingly like one another. Multiple performance measures are produced to validate the prediction that was made by the supervised regression algorithms. The term "performance metrics" refers to that category of metrics. The Gaussian process regression model is the one that produces the most remarkable outcomes when it comes to gain prediction, according to the numerous analyses and results that were obtained. There is complete compatibility between the findings of the simulation and the measurements, and the MIMO antenna that was designed can cover the high band of the 5 G frequency spectrum. The simulation results, measurements, and predictions indicate that the suggested MIMO antenna is suitable for 5 G applications.

CRediT authorship contribution statement

Redwan A. Ananta: Formal analysis, Methodology, Validation. **Md Sharif Ahammed:** Conceptualization, Data curation, Formal analysis, Investigation, Methodology, Writing – original draft. **Md. Ashraful Haque:** Conceptualization, Formal analysis, Investigation, Methodology, Writing – original draft. **Samir Salem Al-Bawri:** Conceptualization, Formal analysis, Funding acquisition, Investigation, Methodology, Project administration, Software, Supervision, Validation, Writing – original draft. **Noorlindawaty Md Jizat:** Funding acquisition, Resources, Writing – review & editing. **Khaled Aljaloud:** Funding acquisition, Resources, Writing – review & editing. **Kamal Hossain Nahin:** Data curation, Methodology, Writing – review & editing. **Wazie M. Abdulkawi:** Resources, Writing – review & editing.

Declaration of Competing Interest

All authors have no conflicts of interest.

Acknowledgments

This research supported by the Researchers Supporting Project number (RSP2024R474), King Saud University, Riyadh, Saudi Arabia.

References

[1] R. Azim, K. Dhar, Md.S. Mia, M.T. Islam, Inset-fed microstrip patch antenna for ubiquitous wireless communication applications, IJUWBCS vol. 5 (2) (2022) 57, https://doi.org/10.1504/IJUWBCS.2022.123416.

[2] L.C. Paul, Md.A. Haque, S. Sarker, Md.M. Ur Rashid, Md.A. Haque, and T.K. Roy, Design and Performance Exploration of a DGS Metamaterial MPA by Etching Four Dual Isosceles Triangular Defects on the Ground Plane, in *2018 International Conference on Computer, Communication, Chemical, Material and Electronic Engineering (IC4ME2)* , Rajshahi: IEEE, Feb. 2018, pp. 1–4. ⟨doi:10.1109/IC4ME2.2018.8465670⟩.

[3] L.C. Paul, et al., A compact wrench-shaped patch antenna with a slotted parasitic element and semi-circular ground plane for 5G communication, e-Prime - Adv. Electr. Eng., Electron. Energy vol. 6 (Dec. 2023) 100334, https://doi.org/10.1016/j.prime.2023.100334.

[4] J. Yeo, J.-I. Lee, Gain enhancement of microstrip patch array antennas using two metallic plates for 24 GHz radar applications, Electronics vol. 12 (7) (Mar. 2023) 1512, https://doi.org/10.3390/electronics12071512.

[5] P. Das, K. Mandal, A. Lalbakhsh, Beam-steering of microstrip antenna using single-layer FSS based phase-shifting surface, Int J. RF Mic. Comp. -Aid Eng. vol. 32 (3) (Mar. 2022), https://doi.org/10.1002/mmce.23033.

[6] A. Sharma, Antenna array pattern synthesis using metaheuristic algorithms: a review, IETE Tech. Rev. vol. 40 (1) (Jan. 2023) 90–115, https://doi.org/10.1080/02564602.2022.2051616.

[7] N.K. Mallat, M. Ishtiaq, A. Ur Rehman, A. Iqbal, Millimeter-Wave in the Face of 5G communication potential applications, IETE J. Res. vol. 68 (4) (Jul. 2022) 2522–2530, https://doi.org/10.1080/03772063.2020.1714489.

[8] N. Sheriff, S. Kamal Abdul Rahim, H. Tariq Chattha, T. Kim Geok, Multiport single element mimo antenna systems: a review, Sensors vol. 23 (2) (Jan. 2023) 747, https://doi.org/10.3390/s23020747.

[9] O. Bello, S. Zeadally, Internet of underwater things communication: architecture, technologies, research challenges and future opportunities, Ad Hoc Netw. vol. 135 (Oct. 2022) 102933, https://doi.org/10.1016/j.adhoc.2022.102933.

[10] M. Khalid, et al., 4-Port MIMO antenna with defected ground structure for 5g millimeter wave applications, Electronics vol. 9 (1) (Jan. 2020) 71, https://doi.org/10.3390/electronics9010071.

[11] S. Sharma, M. Arora, A millimeter wave elliptical slot circular patch mimo antenna for future 5g mobile communication networks, PIER M vol. 110 (2022) 235–247, https://doi.org/10.2528/PIERM22041101.

[12] S. Rahman, et al., Nature Inspired MIMO antenna system for future mmWave technologies, Micromachines vol. 11 (12) (Dec. 2020) 1083, https://doi.org/10.3390/mi11121083.

[13] M. Usman, E. Kobal, J. Nasir, Y. Zhu, C. Yu, A. Zhu, Compact SIW fed dual-port single element annular slot MIMO antenna for 5G mmWave applications, IEEE Access vol. 9 (2021) 91995–92002, https://doi.org/10.1109/ACCESS.2021.3091835.

[14] R. Hussain, et al., A multiband shared aperture MIMO antenna for millimeter-wave and Sub-6GHz 5G applications, Sensors vol. 22 (5) (Feb. 2022) 1808, https://doi.org/10.3390/s22051808.

[15] I. Ud Din, et al., Frequency-selective surface-Based MIMO antenna array for 5g millimeter-wave applications, Sensors vol. 23 (15) (Aug. 2023) 7009, https://doi.org/10.3390/s23157009.

[16] S. Iffat Naqvi, et al., Integrated LTE and millimeter-wave 5G MIMO antenna system for 4G/5G wireless terminals, Sensors vol. 20 (14) (Jul. 2020) 3926, https://doi.org/10.3390/s20143926.

[17] S.M. El-Nady, A.M. Attiya, Periodically-stub-loaded microstrip line wideband circularly polarized millimeter wave MIMO antenna, IEEE Access vol. 10 (2022) 20465–20472, https://doi.org/10.1109/ACCESS.2022.3152222.

[18] A.K. Dwivedi, N.K. Narayanaswamy, K.K.V. Penmatsa, S.K. Singh, A. Sharma, V. Singh, Circularly polarized printed dual port MIMO antenna with polarization diversity optimized by machine learning approach for 5G NR n77/n78 frequency band applications, Sci. Rep. vol. 13 (1) (Aug. 2023) 13994, https://doi.org/10.1038/s41598-023-41302-2.

[19] L.C. Paul, M.A. Haque, M.A. Haque, M.M.U. Rashid, M.F. Islam, and M.M. Rahman, Design a slotted metamaterial microstrip patch antenna by creating three dual isosceles triangular slots on the patch and bandwidth enhancement, in *2017 3rd International Conference on Electrical Information and Communication Technology (EICT)* , Khulna: IEEE, Dec. 2017, pp. 1–6. ⟨doi:10.1109/EICT.2017.8275143⟩.

[20] I. Rahaman, et al., Performance analysis of linearly arranged concentric circular antenna array with low sidelobe level and beamwidth using robust tapering technique, Micromachines vol. 13 (11) (Nov. 2022) 1959, https://doi.org/10.3390/mi13111959.

[21] X. Cao, Y. Xia, L. Wu, X. Wu, Tri-band MIMO antenna design based on characteristic modes manipulation, AEU - Int. J. Electron. Commun. vol. 155 (Oct. 2022) 154318, https://doi.org/10.1016/j.aeue.2022.154318.

[22] Md.A. Haque, L.C. Paul, R. Azim, Md.M. Mowla, A. Saleh, and Md.N. Hossain, A Modified E-Shaped Microstrip Patch Antenna for C Band Satellite Applications, in *2019 IEEE International Conference on Signal Processing, Information, Communication & Systems (SPICSCON)*, Dhaka, Bangladesh: IEEE, Nov. 2019, pp. 27–31. ⟨doi:10.1109/SPICSCON48833.2019.9065126⟩.

[23] M.A. Haque, L.C. Paul, S. Kumar, R. Azim, Md.S. Hosain, and M. Azman Zakariya, A Plowing T-shaped Patch Antenna for WiFi and C Band Applications, in *2021 International Conference on Automation, Control and Mechatronics for Industry 4.0 (ACMI)*, Rajshahi, Bangladesh: IEEE, Jul. 2021, pp. 1–4. ⟨doi:10.1109/ACMI53878.2021.9528266⟩.

[24] N. Bisht, P.K. Malik, S. Das, T. Islam, S. Asha, M. Alathbah, Design of a modified MIMO antenna based on tweaked spherical fractal geometry for 5g new radio (NR) band N258 (24.25–27.25 GHz) applications, Fractal Fract. vol. 7 (10) (Sep. 2023) 718, https://doi.org/10.3390/fractalfract7100718.

[25] A. Ahmad, D. Choi, S. Ullah, A compact two elements MIMO antenna for 5G communication, Sci. Rep. vol. 12 (1) (Mar. 2022) 3608, https://doi.org/10.1038/s41598-022-07579-5.

[26] S. Jayant and G. Srivastava, Four Elements UWB MIMO Antenna Array, in *2020 7th International Conference on Signal Processing and Integrated Networks (SPIN)*, Noida, India: IEEE, Feb. 2020, pp. 48–54. ⟨doi:10.1109/SPIN48934.2020.9070922⟩.

[27] K.S. Sultan, H.H. Abdullah, Planar uwb mimo-diversity antenna with dual notch characteristics, PIER C. vol. 93 (2019) 119–129, https://doi.org/10.2528/PIERC19031202.

[28] A.H. Jabire, et al., Metamaterial based design of compact UWB/MIMO monopoles antenna with characteristic mode analysis, Appl. Sci. vol. 11 (4) (Feb. 2021) 1542, https://doi.org/10.3390/app11041542.

[29] L. Malviya, R.K. Panigrahi, M.V. Kartikeyan. MIMO Antennas for Wireless Communication: Theory and Design, 1st ed, CRC Press, 2020, https://doi.org/10.1201/9781003080275.

[30] A. Haque, et al., Design and analysis of sphere yagi antenna at 915 MHz Band for LoRaWAN application, J. Phys.: Conf. Ser. vol. 2550 (1) (Aug. 2023) 012015, https://doi.org/10.1088/1742-6596/2550/1/012015.

[31] L.C. Paul, M.S. Akhter, M.A. Haque, M.R. Islam, M.F. Islam, and M.M. Rahman, Design and analysis of four elements E, H and combined E-H shaped microstrip patch array antenna for wireless applications, in *2017 3rd International Conference on Electrical Information and Communication Technology (EICT)* , Khulna: IEEE, Dec. 2017, pp. 1–6. ⟨doi:10.1109/EICT.2017.8275141⟩.

[32] M.S. Yahya, S. Soeung, S.K.A. Rahim, U. Musa, S.S. Ba Hashwan, Md.A. Haque, Machine learning-optimized compact frequency reconfigurable antenna With RSSI enhancement for long-range applications, IEEE Access vol. 12 (2024) 10970–10987, https://doi.org/10.1109/ACCESS.2024.3355145.

[33] Md.A. Haque, et al., Dual band antenna design and prediction of resonance frequency using machine learning approaches, Appl. Sci. vol. 12 (20) (Oct. 2022) 10505, https://doi.org/10.3390/app122010505.

[34] Md.A. Haque, et al., Machine learning-based technique for gain and resonance prediction of mid band 5G Yagi antenna, Sci. Rep. vol. 13 (1) (Aug. 2023) 12590, https://doi.org/10.1038/s41598-023-39730-1.

[35] W.-H. Chen, et al., Forecast of glucose production from biomass wet torrefaction using statistical approach along with multivariate adaptive regression splines, neural network and decision tree, Appl. Energy vol. 324 (Oct. 2022) 119775, https://doi.org/10.1016/j.apenergy.2022.119775.

[36] D. Borup, B.J. Christensen, N.S. Mühlbach, M.S. Nielsen, Targeting predictors in random forest regression, Int. J. Forecast. vol. 39 (2) (Apr. 2023) 841–868, https://doi.org/10.1016/j.ijforecast.2022.02.010.

[37] A. Caron, G. Baio, I. Manolopoulou, Estimating individual treatment effects using non-parametric regression models: a Review, J. R. Stat. Soc. Ser. A: Stat. Soc. vol. 185 (3) (Jul. 2022) 1115–1149, https://doi.org/10.1111/rssa.12824.

[38] R. Wang, L. Wang, J. Zhang, M. He, J. Xu, Xgboost machine learning algorism performed better than regression models in predicting mortality of moderate-to-severe traumatic brain injury, World Neurosurg. vol. 163 (Jul. 2022) e617–e622, https://doi.org/10.1016/j.wneu.2022.04.044.

[39] Md.A. Haque, et al., Machine learning-based technique for resonance and directivity prediction of UMTS LTE band quasi Yagi antenna, Heliyon vol. 9 (9) (Sep. 2023) e19548, https://doi.org/10.1016/j.heliyon.2023.e19548.

[40] G. Zhou, G. Hu, D. Zhang, Y. Zhang, A novel algorithm system for wind power prediction based on RANSAC data screening and Seq2Seq-Attention-BiGRU model, Energy vol. 283 (Nov. 2023) 128986, https://doi.org/10.1016/j.energy.2023.128986.

[41] M.A. Rahman, S.S. Al-Bawri, W.M. Abdulkawi, K. Aljaloud, M.T. Islam, A unique SWB multi-slotted four-port highly isolated MIMO antenna loaded with metasurface for IOT applications-based machine learning verification, Eng. Sci. Technol., Int. J. vol. 50 (Feb. 2024) 101616, https://doi.org/10.1016/j.jestch.2024.101616.

[42] Md.A. Haque, et al., Quasi-Yagi antenna design for LTE applications and prediction of gain and directivity using machine learning approaches, Alex. Eng. J. vol. 80 (Oct. 2023) 383–396, https://doi.org/10.1016/j.aej.2023.08.059.

[43] M. Ashraful Haque, et al., Machine learning-based approach for bandwidth and frequency prediction for N77 band 5G antenna, Phys. Scr. vol. 99 (2) (Feb. 2024) 026005, https://doi.org/10.1088/1402-4896/ad1d40.